Natural Hazards (2025) 121:17439–17469
https://doi.org/10.1007/s11069-025-07478-8

ORIGINAL PAPER

Statistically-based regional landslide susceptibility assessment in the UNESCO global geopark Caminhos dos Cânions do Sul (Brazil)

Marina Tamaki de Oliveira Sugiyama[1] · José Eduardo Bonini[1] · Tiago Damas Martins[2] · Maria Carolina Villaça Gomes[3] · Susana Pereira[4,5] · Bianca Carvalho Vieira[1]

Received: 9 January 2025 / Accepted: 16 June 2025 / Published online: 2 July 2025

Abstract
The scenic value of landscapes within Geoparks is often attributed to the geomorphological processes that have shaped them in the past or up to the present day, including landslides. However, these processes also pose significant threats to the integrity of geosites and the safety of visitors, highlighting the need for risk prevention and mitigation plans for geohazards. The Caminhos dos Cânions do Sul Geopark (southern Brazil) lacks landslide inventories and susceptibility maps, essential for conducting practical geohazard risk analyses. This study addresses this gap by compiling a landslide inventory of the major events over the past 30 years, using a rule-based Object-Based Image Analysis (OBIA) approach, and assessing the susceptibility for four modeling domains within the Geopark using the Information Value method. Seven independent variables (aspect, slope, topographic wetness index, terrain ruggedness index, geomorphons, elevation, and curvature) were selected, resulting in 120 combinations for each modeling domain. For each predisposing factor combination, model performance was assessed using the area under the Receiver Operating Characteristics (ROC) curve, and the conditional independence of variables was evaluated. The best models for each domain were selected based on the criteria of conditional independence, goodness of fit, and number of variables. The final landslide susceptibility map was produced by merging the best three models' results. The resulting susceptibility classification indicates that many geosites are located in areas with moderate to very high susceptibility or within zones likely to experience material transport or deposition.

Keywords Global Geoparks Network · Serra Geral Escarpment · Object-based image analysis · Information value method

Extended author information available on the last page of the article

1 Introduction

UNESCO Global Geoparks are unified and well-delimited areas managed through a holistic economic and social sustainable development concept, with geotourism as its main driving activity (Jones 2008; Brilha 2018; Lee and Jayakumar 2021). Global Geoparks harbor important geosites, representing unique geological features, landscapes, and cultural heritage that should be preserved for future generations (Reynard 2009). Geoparks can be considered an outstanding initiative in promoting geosite conservation (Brilha 2018). Despite its role as a source of leisure, education, and income for its community, Geoparks' landscapes can also pose hazardous situations for their visitors and inhabitants, particularly in areas with scenic value associated with active geomorphological processes (e.g., mass movements) (Dierickx et al. 2016; Reynard and Coratza 2016; Morino et al. 2022).

As with other UNESCO heritage sites, many of the global geoparks comprise areas prone to natural hazards and extreme weather events (Fukuoka 2014; Pavlova 2019). A survey with UNESCO geopark managers shows that landslides are present in 70% of the geoparks and represent one of the most frequent processes in these territories that can lead to risk situations (Dierickx et al. 2016). Therefore, in addition to the necessity to assess risk and create prevention and mitigation plans due to the natural characteristics of these territories, UNESCO geoparks can help countries achieve the Sustainable Development Goals (SDGs) of the 2030 Agenda and the Shimbara Declaration to ensure safe and resilient cities and prevent impacts caused by natural processes (EGN 2012; UN 2018; Fassoulas et al. 2018).

The UNESCO Global Geopark Caminhos dos Cânions do Sul (henceforth GCCS), located in Southern Brazil, has an area of approximately 3.000 km² and the occurrence of geomorphological processes deeply marks the landscape. Whether on its outstanding basaltic escarpment (Serra Geral) or its vast plains, it is possible to attest the power of these landscape-shaping processes, especially mass movements (shallow landslides, rockfalls, and debris flows), floods, and flash floods (Pellerin et al. 1997; Valdati et al. 2021; Vasconcellos et al. 2021; Paixão et al. 2021; Szymasnki et al. 2022; Sugiyama and Gomes 2023). Although this area has always been a popular tourist destination in the region, establishing the GCCS increased the region's appeal for geotourism, leading to the installation of new infrastructure and a boost in the number of visitors. This situation prompted the necessity for geohazard risk prevention and mitigation plans.

However, landslide risk assessments can be time- and resource-consuming, especially for large areas such as geoparks, because they involve a series of preceding steps (e.g., susceptibility, hazard, and vulnerability analysis) (Van Westen et al. 2008). The first step to assess landslide risk can be the susceptibility assessment, defined in this research as the analysis of landslide spatial probability in an area, considering only the terrain characteristics (Brabb 1984; Guzzetti et al. 1999). Given that scale is a critical factor when selecting the most appropriate method for susceptibility assessments, statistical methods are recommended in the literature for regional-scale analysis across large areas due to the necessity of detailed information on the physical properties of soils and rocks for the use of physically-based models (Soeters and van Westen 1996; Aleotti and Chowdhury 1999; Reichenbach et al. 2018).

One of the major advantages of statistical methods is that the investigator can validate the importance of the predisposing factors and decide on the input of the final maps (Aleotti and Chowdhury 1999; Corominas et al. 2014). Nevertheless, when modeling landslide sus-

ceptibility across large areas, the spatial variability of lithological, geotechnical, and topographic characteristics should be considered (Lee et al. 2008; Blahut et al. 2010; Petschko et al. 2014). Distinct approaches for modeling heterogeneous domains have been proposed, mainly based on subdivisions of the area in relatively topographically homogeneous sectors (Lee et al. 2008; Blahut et al. 2010) and lithologically homogeneous domains at a given scale (Petschko et al. 2012, 2014).

For some GCCS municipalities (namely, Jacinto Machado and Timbé do Sul), previous research was carried out with bivariate statistically-based methods to understand landslide susceptibility with municipal planning and civil protection purposes (IPT, 2015a, b). Furthermore, other studies analyzed mass movement hazard through physically-based methods in touristic areas of the GCCS (e.g., Franck and Kobiyama 2024). However, although some punctual qualitative efforts to recognize potential geohazards in the whole GCCS territory were made (Pimenta et al. 2018; Sugiyama and Gomes 2023), systematic landslide inventories and quantitative susceptibility mapping are still lacking, specifically focused on Geopark management. Statistically-based susceptibility assessments critically rely on landslide inventories that should be as complete and unbiased as possible (Dikau et al. 1996; Aleotti and Chowdhury 1999; Ardizzone et al. 2002), a type of dataset lacking for the GCCS territory, and that limits the application of regional-scale statistically based models.

The visual interpretation of aerial photography and/or orbital images is the most common technique for producing geomorphological inventories (Galli et al. 2008; Bucci et al. 2021; Zhang et al. 2022). However, these techniques may be time-consuming when mapping large areas or producing multi-temporal inventories, and, in recent decades, various studies have employed automatic and semiautomatic methodologies, such as Object-based image analysis (OBIA) techniques, reducing reliance on visual interpretation (Lacroix et al. 2013; Amatya et al. 2021; Meena et al. 2021). Although not entirely objective, semiautomatic methods can be a time-saving tool for large and heterogeneous areas once training sample collection is optional.

Therefore, this paper aims to produce a regional-scale statistically-based susceptibility assessment for the GCCS, capable of depicting the differences in landslide susceptibility and its predisposing factors across the different geomorphological domains that characterize the Geopark landscape. For this purpose, a set of landslide inventories of the major events that occurred in the last 30 years in the GCCS was produced by using archive satellite imagery and the OBIA technique. These products can contribute to establishing geohazard risk prevention and mitigation plans in the GCCS by providing the two essential products (inventories and susceptibility maps) necessary for a future quantitative landslide risk assessment.

2 Study area

The UNESCO GCCS is located in southern Brazil, spanning seven municipalities (Morro Grande, Timbé do Sul, Jacinto Machado, Praia Grande, Torres, Mampituba and Cambará do Sul) across two states (Rio Grande do Sul and Santa Catarina) (Fig. 1). The geological framework of GCCS reflects a series of geotectonic events related to the formation of the Paraná-Etendeka Basin and the breakup of the Gondwana Supercontinent, which occurred from the Ordovician to the Late Cretaceous (Milani et al. 2007). The primary geological

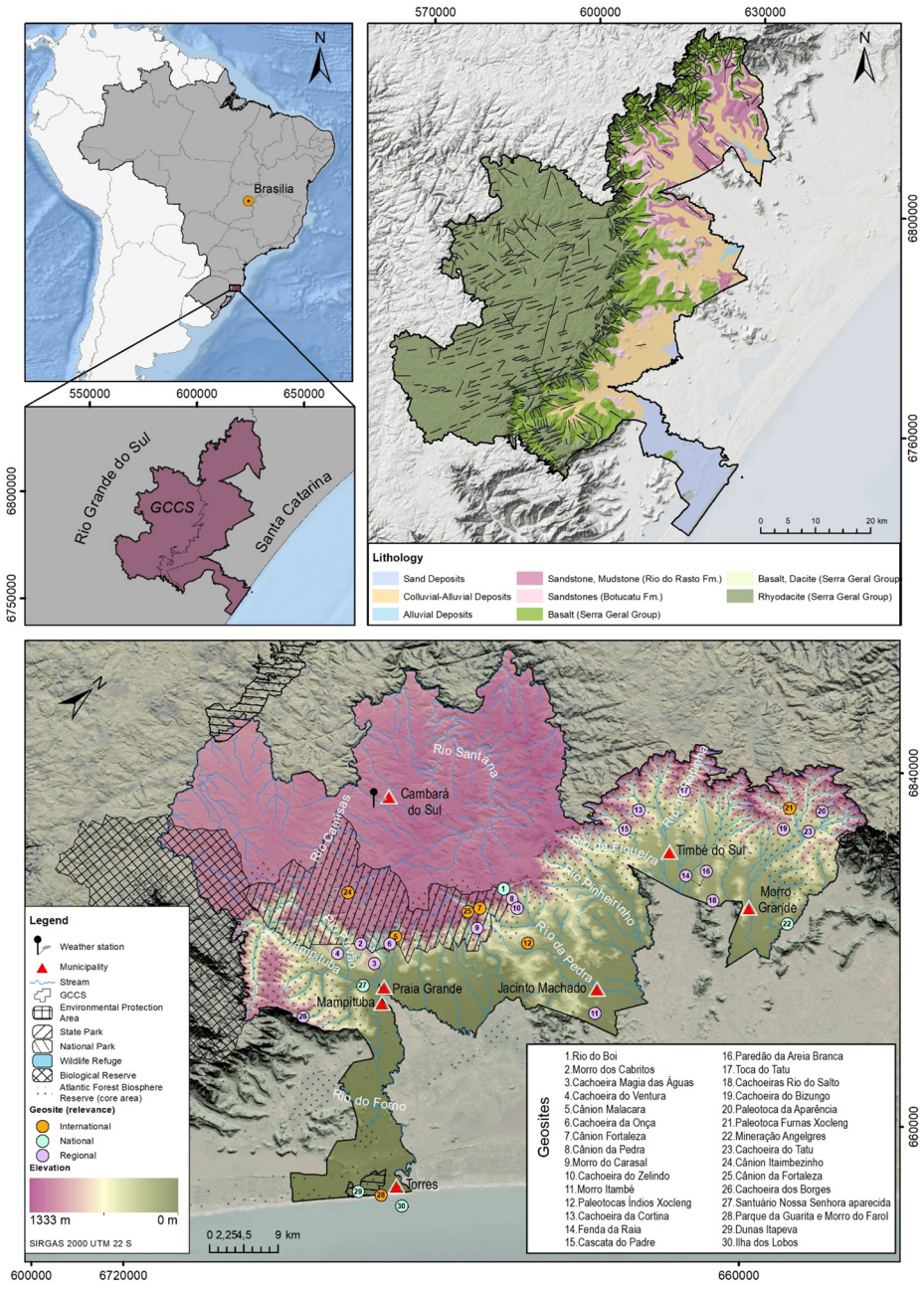

Fig. 1 Lithological map of the study area, nature conservancy units, geosites, and weather station of the GCCS

units of this volcano-sedimentary basin are, in stratigraphic order from bottom to top, the Upper Permian Rio do Rasto Formation (comprising tabular sandstones interbedded with mudstones), the Upper Jurassic to Lower Cretaceous Botucatu Formation (medium-thickness red sandstones), and the Cretaceous Serra Geral Formation Group (including basalt, rhyodacite, and dacite) (Wildner et al. 2008, 2014).

Erosional processes acting on these lithologies have led to the formation of four distinct geomorphological domains: (1) the Campos Gerais Highlands, located above 1,000 m in elevation, which are supported by magmatic rocks and characterized by an intense structural control over the drainage system, with predominant flat surfaces; (2) the Serra Geral Escarpment, which marks the edge of the highlands and are also sustained by lithologies of the Serra Geral Group, presenting steep slopes and numerous joints and fractures; (3) the Serra Geral Patamares, a step-like relief formed by sedimentary rocks (Botucatu and Rio do Rasto formations) that connect the highlands and escarpment to the plains; and (4) the coastal plains, which are composed of tertiary and quaternary sediments, resulting from colluvial, fluvial, and coastal processes.

The geodiversity of this region is recognized through 30 official geosites, eight of which are of international significance (Fig. 2). These include canyons, waterfalls, paleoburrows, rock outcrops, and other distinctive landforms. Additionally, the GCCS encompasses 11 nature conservation units (Fig. 1), highlighting its rich biotic and cultural diversity.

The municipalities of the GCCS are generally sparsely populated. According to the 2022 demographic census, the municipality with the largest and most densely occupied population is Torres (41,751 inhabitants, 258 inhabitants/km²). The second most populous municipality is Jacinto Machado (10,624 inhabitants), while the other municipalities have populations of less than 10,000 inhabitants, such as Morro Grande and Mampituba, with approximately 3,000 inhabitants.

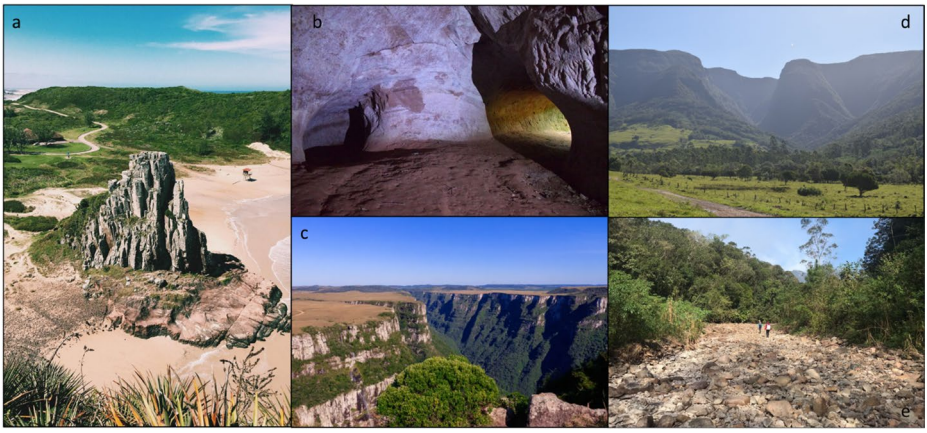

Fig. 2 (**a**) Geosite Morro do farol, an outcrop of Serra Geral Group and Botucatu Formation, displaying a singular lithology (peperites) formed by the interaction between the sands of the ancient desert (Botucatu) and the volcanic flows; (**b**) Geosite Toca do Tatu, a paleoburrow dug into Botucatu sandstones; (**c**) Geosite Canion da Fortaleza, a canyon developed through the fractures of the basaltic rocks, on which different basaltic flows are visible; (**d**) The landscape of the GCCS is marked by the presence of the Serra Geral Escarpment, with considerable elevation range; (**e**) evidence of hydrodynamic processes on the plains. Source: (**c**) Yasmim Fontana

The presence of the escarpment, with an elevation range of more than 1,000 m, significantly influences rainfall patterns, promoting the occurrence of orographic precipitation. In the GCCS, the average annual rainfall is 1,823 mm, as recorded at a weather station located in the highlands. However, no weather station exists on the escarpment itself. Previous studies have shown a 30% increase in annual rainfall over a vertical distance of just 150 m (from 70 to 220 m), with 2,519 mm recorded at 220 m (Valdati 2000). Consequently, persistent rainfall in the headwaters is not uncommon, often resulting in generalized hydrodynamic processes and landslides (Fig. 2). A notable example of this is the 1995 rainfall event, which triggered hundreds of landslides and debris flows, leading to the loss of 29 lives (Pellerin et al. 1997).

3 Materials and methods

3.1 Data and software

Different data sources were used to produce the landslide inventories and susceptibility maps. For the inventories, SPOT (*Satellite pour l'Observation de la Terre*) and RapidEye archive images were used. Images were made available in the frame of the CNES SPOT World Heritage Programme and the Planet Education and Research Program (Planet Team 2017), respectively. Elevation data (30 m spatial resolution) was derived from the Forest and Buildings Removed Copernicus Digital Elevation Model version 1.2 (DEM) (Hawker et al. 2022), used both during the inventory production and susceptibility modeling steps.

The most detailed geological map for the study area is available at a 1:500,000 scale, and using this product to define modeling domains could lead to oversimplified results (Wildner et al. 2008, 2014). Nevertheless, a geomorphological map at a 1:250,000 scale is available (IBGE, 2023) and was used to determine the three modeling domains (highland, escarpment, and plains) for the landslide susceptibility modeling. The abovementioned map was produced by a systematic field survey and geomorphological interpretation of orbital imagery, resulting in a standardized product for the Brazilian territory. The geomorphological units comprise landforms with altimetric and physiographic resemblance due to similar lithological, tectonic, and paleoclimatic histories (IBGE 2009).

All processes were performed by SAGA GIS (Conrad et al. 2015) and the R statistical software (R Core Team 2019). We used custom functions in the R language for variable weighting, evaluation of model fit, and conditional independence diagnosis. The latter was based on Agterberg and Cheng (2002), and the code implemented in ArcSDM (Sawatzky et al. 2009), available at https://github.com/gtkfi/ArcSDM/tree/master.

3.2 Landslide inventory mapping

The generalized events were identified from official registers (in the case of the 1995 event) and the visual analysis of multitemporal orbital imagery available on Google Earth. When landslides were identified on a given date, SPOT and RapidEye databases were queried to acquire post-event imagery (Table 1). Three major events were identified inside the Geopark territory, one with the precise triggering date reported and two with uncertain triggering dates (the first triggered between 2005 and 2007, and the second between 2009 and 2011).

Table 1 Remote sensing data for the landslide inventories

	Platform and sensor	Spatial resolution	Acquisition date
Inventory I	SPOT3, HRV (High-Resolution Visible)	10 m	06/04/1996
Inventory II	RapidEye, MSI (Multispectral Imager)	5 m	05/05/2007
Inventory III	RapidEye, MSI	5 m	21/09/2011

Remote sensing data (Table 1) was processed to obtain local statistical measures from the post-event images (contrast, entropy, energy, and variance) (Zhang 2011) and morphometric terrain attributes were derived from the DEM (catchment area, slope, topographic wetness index, aspect, curvature, and geomorphons).

The approach for landslide inventory mapping was based on a two-level Object-Based Image Analysis (OBIA) using the seeded region growing algorithm (Adams and Bischof 1994). The first segmentation was performed at a coarser level (i.e., with a larger bandwidth value), aimed at removing areas not affected by landslides and with homogeneous land cover. After removing the non-affected areas, a fine-level segmentation was performed using smaller bandwidth values to refine landslide polygon borders. Landslides were differentiated from non-affected regions at both levels using a rule-based classification. Rules were based on local statistical measures and DEM derivatives (mean and standard deviation for both) and defined from manually digitized landslide polygons inside a 1.5 km² area (one area per inventory). After the fine-level segmentation and classification, a preliminary inventory was obtained and compared to the manually digitized landslides with a confusion matrix to obtain the proportion of true positives (TP), true negatives (TN), false positives (FP), false negatives (FN), user and producer accuracies, and overall accuracy. User accuracy (UA) (Eq. 1) refers to the commission error and denotes the proportion of pixels correctly classified in a given class. Producer accuracy (PA) (Eq. 2) is related to the omission error and denotes the proportion of correctly identified landslides from the manual inventory. Overall accuracy (OA) (Eq. 3) is the proportion of correctly identified classes across the analyzed data (i.e., considering both landslides and non-landslides).

$$UA = \frac{TP}{TP + FP} \tag{1}$$

$$PA = \frac{TP}{TP + FN} \tag{2}$$

$$OA = \frac{(TP + FN)}{(TP + TN + FP + FN)} \tag{3}$$

.

Afterward, false positives were removed, landslide polygon borders were corrected when necessary, and non-detected landslides were manually digitized. A further classification of the preliminary inventory was performed using the geomorphons layer to differentiate areas affected by shallow landslides on the slopes and valley bottoms affected by debris flows and other hydrodynamic processes (hereafter, landslides refer to shallow translational landslides). We considered a given landslide polygon to be affected by debris flows and other

hydrodynamic processes if its overlaid areas were classified as valley geomorphons. Landslide polygons in other geomorphons were considered shallow landslides, rupture, transport, and deposition zones, mapped as a single polygon. After this step, a further visual interpretation was carried out to ensure the consistency of the separation process. Landslide initiation points were automatically derived from the DEM for each shallow landslide polygon, assuming the initiation point as the highest elevation pixel inside each polygon (Amatya et al. 2022). Finally, the initiation points were randomly partitioned into two subsets (training and test), each with 50% of the landslide population. The initiation points were used in the susceptibility analysis as the pixel corresponding to the location of the initiation point in vector format.

3.3 Modeling of heterogeneous areas

Based on the geomorphological units the GCCS territory was subdivided into four different areas for modeling purposes: (1) Total Area (TA); (2) Highland and Escarpment Area (HSA); (3) Plains and Escarpment Area (PLSA); and (4) Escarpment Area (SA) (Fig. 3). Although the Serra Geral Patamares is delimited separately in the official map, its characteristics are similar to those of the escarpment, especially regarding the geomorphological processes. Therefore, they were included in the escarpment (SA) modeling domain.

Considering that the landslide initiation points occur on the escarpment area, the escarpment area was necessarily included in all subdivisions. Based on the geomorphological units, the subdivision aimed to analyze whether the construction of a model for the whole area would be satisfactory or if the modeling based on different domains would generate more fitted results for Geopark management.

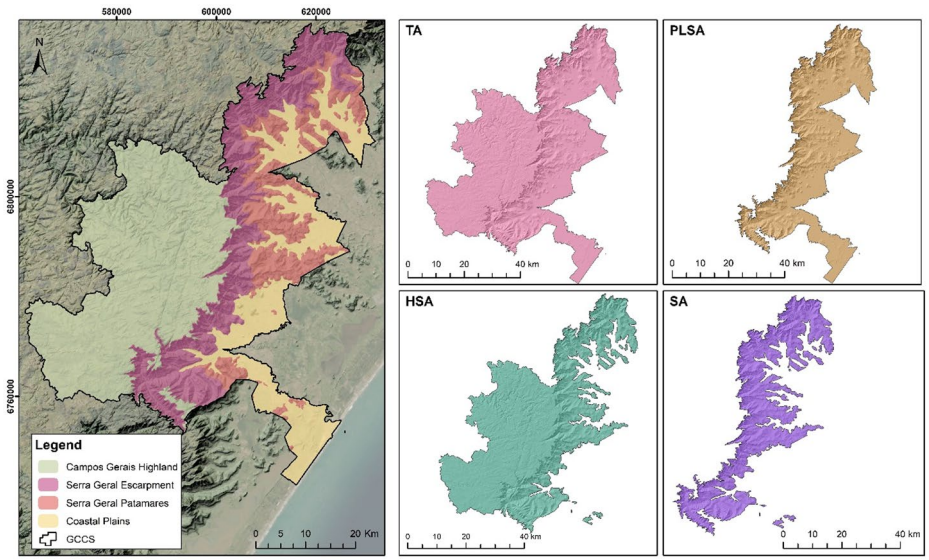

Fig. 3 Geomorphological compartments and modeling domains (TA = Total Area; PLSA = Plains and Escarpment Area; HSA = Highland and Escarpment Area; SA = Escarpment Area)

3.4 Predisposing factors

Predisposing factors were derived from the Digital Elevation Model (DEM) and comprised seven morphometric parameters (Table 2). The selection of predisposing factors and their categorization were based on our knowledge of the study area and the literature about landslide controlling factors (Table 2). The option to include only topography-related variables in the models is justified by the modeling in heterogeneous domains, whose limits are intrinsically related to lithological and tectonic controls.

3.5 Susceptibility modeling and validation

The Information Value (Yin and Yan 1988) was deployed to weigh each class of the predisposing factors. The Information Value (IV) of a class *i* of a predisposing factor *x* is given by the relation of the landslide-affected area in class *i* (S_i), the area of class *i* (N_i), the total landslide-affected area (S), and the total area (N) (Eq. 4).

$$IV_{xi} = \ln \frac{S_i / N_i}{S / N} \tag{4}$$

Table 2 Selected predisposing factors for the susceptibility analysis

Predisposing factor (unit)	Brief rationale for selection	
Aspect (degrees)	It can be a proxy for slope morpho-structural properties (e.g., dip angle). It can also influence moisture content due to differential exposure to rainfall and/or solar radiation.	Corominas et al. (2014) Messenzehl et al. (2017) Zêzere et al. (2017)
Slope angle (degrees)	The determinant factor for landslide triggering. Theoretically, shear stress increases with increasing slope angle.	Bierman and Montgomery (2019), McColl (2015)
Geomorphons (-)	Differentiates landforms that can be associated with landslide deposition zones (e.g., depressions and valleys) and rupture zones (e.g., hollows and slopes).	Steger et al. (2021) Zhang et al. (2020)
Curvature (-)	Indicator of slope hydrology, with a tendency of flow convergence in concave slopes and divergence in convex ones.	Dietrich and Montgomery (1998); Lacerda (2007)
Elevation (m)	Can exert influence due to the increase in potential energy as a result of the elevation difference	Corominas et al. (2014)
Terrain Ruggedness Index (TRI) (-)	Indicate relief heterogeneity, which can reflect differences in potential energy, similarly to elevation, but considering neighboring mapping units.	Corominas et al. (2014); Bordoni et al. (2020)
Topographic Wetness Index (TWI) (-)	It can be considered a proxy for slope moisture retention and saturation zones.	Beven and Kirby (1979) Seibert et al. (2007)

.

When the IV of a class *i* assumes negative values, the class is not useful in explaining the landslide distribution, and it can be assumed that it is favorable to slope stability (Zêzere et al. 2017). Conversely, when the IV of class *i* is positive, variable *xi* is relevant to explain the landslide distribution (with higher positive values indicating higher association) (Pereira et al. 2012; Zêzere et al. 2017). If landslides are absent in a given class *xi*, Eq. 1 cannot be computed. In such cases, the IV was set to the lowest IV obtained for the predisposing factor *x*, subtracted by 0.001. The final IV is determined by the sum of all thematic maps, with each class reclassified according to its IV. The weighting of the predisposing factors was performed using the landslide training subset.

After computing the IV of each variable *xi*, model fit was evaluated independently with the training subset for all possible combinations of predisposing factors. For each modeling domain, 120 combinations were computed, resulting in 480 models. The rationale of this combination procedure was to provide insights into potential differences in the main landslide-controlling factors in each modeling domain. Model fit was evaluated for each model using the Receiver Operating Characteristics area under the curve (ROC AUC) (Swets 1988; Bradley 1997; Fawcett 2006). ROC curves relate the sensitivity and the false positive rate derived from contingency matrices computed with different cutoff values (Frattini et al. 2010). ROC AUC represents the overall model accuracy, with values ranging from 0.0 (the model classifies all mapping units as either false positive or false negative) to 1.0 (perfect prediction); a 0.5 value indicates that the model is not better than a random prediction (Swets, 1988; Bradley 1997). In the literature, ROC AUC as a model fit metric tends to be ranked as poor fit (values under 0.7); fair (0.7 to 0.8); good (0.8 to 0.9); and excellent (0.9 or higher) (Fressard et al. 2014).

3.6 Conditional independence diagnosis

Bivariate statistical models assume the existence of conditional independence between the landslide predisposing factors (Bonham-Carter et al. 1989; Van Westen 1993), and the violation of this assumption can lead to overestimations of landslide spatial probability. (Blahut et al. 2010; Pereira et al. 2012). Therefore, conditional independence in the abovementioned 480 combinations was assessed with the Agterberg-Cheng Conditional Independence Test (ACCIT) (Agterberg and Cheng 2002). The ACCIT evaluates the presence of conditional independence based on the predicted training points (*T*) and the actual observed occurrences (*n*), applying a one-tailed test of the null hypothesis that $T\text{-}n=0$. Following Pereira et al. (2012), the posterior probabilities and their standard deviation for each of the predisposing factor classes were obtained by the Weights of Evidence. (Bonham-Carter 1994) and the ACCIT was scaled from 0 to 1. An ACCIT value lower than 0.40 indicates high conditional dependence among the predisposing factors and that the model should be rejected. The aforementioned posterior probability values were obtained using the landslide initiation points of the training subset described in the inventory mapping section.

3.7 Selection of the best landslide susceptibility models

For each modeling domain, the best model was selected based on model fit and whether the hypothesis of conditional independence could be accepted. By the best model, we con-

sidered those with ACCIT above 0.40 and a higher AUC ROC. In the case of models that satisfy the conditional independence hypothesis and have very similar values of AUC ROC, the best model was considered to be the one with fewer variables (Pereira et al. 2012). The selected models were then subject to a predictive capacity assessment using the test subset of the landslide inventory, containing 50% of the occurrences. Predictive capacity was assessed through the area under the prediction rate curve. (Chung and Fabbri 1999, 2003), a plot that relates the proportion of correctly classified landslides and the proportion of the study area predicted as susceptible.

After establishing model predictive skills, the landslide susceptibility maps were classified into 10 classes containing an equal number of terrain units to perform the visual comparison. Following Vakhshoori and Zare (2018), to compute the final map, each selected model was classified into five susceptibility classes (Very Low, Low, Moderate, High, and Very High), corresponding, respectively, to 40%, 20%, 20%, 10%, and 10% of its modeled area. This approach was chosen instead of using equal-area classification (e.g., 20% for each class) to avoid overestimating the extent of very high susceptibility zones. Afterwards, the final landslide susceptibility map for the entire territory of the Geopark was obtained by merging the individual susceptibility maps, already classified, of the three subdivided models (HSA30, PLSA65, SA30). Once the escarpment area was present in all three models, the final model was constructed utilizing only one geomorphological compartment from each modeling area (e.g., only the results of the highland area from the selected HSA model were displayed in the final map).

4 Results

4.1 Landslide inventories

A total area of 1.437 km² was inventoried using a rule-based classification of satellite imagery, and 19,36 km² of mass movement areas were identified (Fig. 4). *Inventory I* has the largest affected area (14,6 km²), and the overall accuracy is 88,89%. In contrast, for *Inventory II* and *Inventory III*, respectively, the affected area was 2,19 km² and 2,57 km², and overall accuracies of 97,23% and 98,39% (Table 3). The classification could identify most mass movement-affected areas, and non-detected areas related mostly to the shade of the slopes and small and elongated scars. Manually removed false positives were associated with agriculture in the plains areas and rock outcrops on the escarpment.

After separating the mass movement types, we identified 12,2 km² and 7,13 km² affected by debris flows and other hydrodynamic processes and landslides, respectively. The mass movement events mapped in Inventory II and Inventory III also affected areas outside the Geopark's boundary in three different municipalities (Siderópolis, Nova Veneza, and Morrinhos do Sul). Therefore, these areas were not included in the modeling steps. Thus, considering only the landslides inside the Geopark, 667 initiation points were automatically extracted from the DEM corresponding to the highest elevation pixel inside each landslide polygon. Only 666 points were considered and partitioned into equal training and test subsets (333 points each).

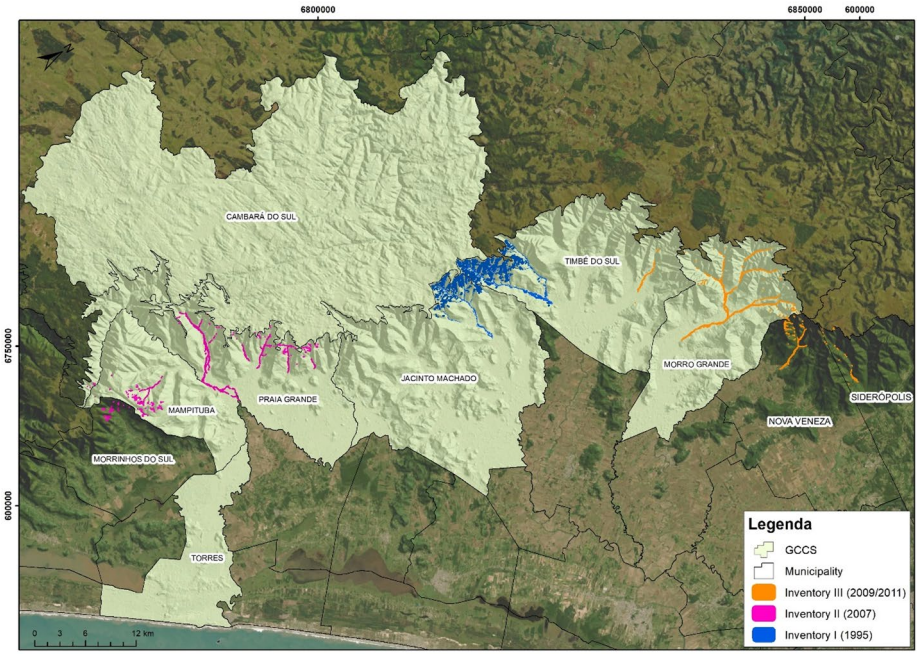

Fig. 4 Landslide inventories of 1995, 2005/2007, and 2009/2011 events

Table 3 Landslide-affected area and accuracies for each inventory

	Landslide-affected area (km²)	Debris flow and other hydrodynamic processes affected area (km²)	User Accuracy (%)	Producer Accuracy (%)	Overall Accuracy (%)
Inventory I	6,62	7,98	73,99	60,61	88,89
Inventory II	0,37	1,82	83,78	64,75	97,23
Inventory III	1,48	2,43	89,19	63,44	98,39

4.2 Information value method

For all the different modeling domains (TA, HAS, PLSA, SA), the class of slope angle that presented the highest information value is the one above 45°. However, the classes between 30° and 45° also show high values (Table 4). North, Northeast, and East-facing slopes presented the highest information values (IV); for TA and HSA, the highest value is for the East aspect, whereas for PLSA and SA, it is Northeast. Flat areas and the Southwest aspect bear a weak relation with the landslide distribution, displaying negative values.

Almost all curvature classes exhibited positive values, indicating some relation with the landslide distribution, except for straight/straight curvatures for TA. The convex/concave curvatures displayed the highest IV for all the modeling domains. The information values of the elevation were higher for TA and HSA in the class from 600 to 800 m, while for PLSA and SA, the most important classes related to landslide distribution were the ones ranging

Table 4 Information values for each predisposing factor and modeling domain. Classes with the highest information value are highlighted in bold type

Predisposing factor	Class	TA	HSA	PLSA	SA
Slope angle (degrees)	< 15	-3.545	-3.234	-3.148	-1.890
	15–20	-0.418	-0.403	-0.608	-0.180
	20–25	0.698	0.707	1.221	1.180
	25–30	1.935	1.940	2.077	2.029
	30–35	2.531	2.533	2.530	2.580
	35–40	2.877	2.877	2.965	2.975
	40–45	2.945	2.945	3.049	3.083
	> 45	**3.330**	**3.330**	**3.482**	**3.401**
Aspect (-)	N	1.126	1.257	1.956	2.273
	NE	1.386	1.616	**1.999**	**2.383**
	E	**1.416**	**1.776**	1.717	2.257
	SE	0.604	0.951	0.881	1.524
	S	0.309	0.525	0.557	0.913
	SW	-0.703	-0.602	-0.836	-0.534
	W	-0.703	-0.602	0.624	0.800
	NW	0.977	1.086	1.687	2.048
	Flat	-0.703	-0.602	-0.836	-
Curvature (-)	V/V	1.159	1.173	1.748	1.795
	R/V	1.576	1.598	2.280	2.274
	X/V	**2.058**	**2.065**	**2.591**	**2.640**
	V/R	0.334	0.410	1.031	1.254
	R/R	-0.383	0.151	0.083	1.313
	X/R	1.154	1.183	1.911	1.981
	V/X	1.219	1.248	1.521	1.637
	R/X	1.282	1.317	1.876	1.913
	X/X	1.448	1.488	2.051	2.104
Elevation (m)	< 200	-0.652	-0.628	-0.167	-0.143
	200–400	-0.652	-0.628	-0.166	-0.143
	400–600	1.950	1.950	2.009	1.992
	600–800	**2.776**	**2.776**	2.814	2.847
	800–1000	0.840	0.840	**3.135**	3.083
	1000–1200	0.287	0.287	3.094	**3.137**
	> 1200	1.843	1.852	1.835	1.766
Geomorphons (-)	Flat	-1.588	-1.570	-1.525	-1.411
	Summit	-1.588	-1.570	-1.525	-1.411
	Ridge	1.382	1.394	1.884	1.896
	Shoulder	-1.588	-1.570	-1.278	-1.235
	Spur	**2.354**	**2.365**	**2.569**	**2.550**
	Slope	1.843	1.854	2.047	2.069
	Hollow	1.818	1.821	2.010	2.078
	Footslope	-1.551	-1.502	-1.525	-1.411
	Valley	-0.975	-0.974	0.410	0.004
	Depression	-1.588	-1.570	-1.525	-1.411

Table 4 (continued)

Predisposing factor	Class	TA	HSA	PLSA	SA
Terrain Ruggedness Index (TRI) (-)	0–0,92	-2.611	-2.579	-2.034	-1.445
	0,92 − 3,69	-2.611	-2.579	-2.034	-1.445
	3,69 − 6,46	1.429	1.437	1.656	1.621
	6,46 − 9,24	2.706	2.708	2.780	2.808
	> 9,24	**3.184**	**3.184**	**3.295**	**3.273**
Topographic Wetness Index (TWI)	2,93 − 4,57	**3.136**	**3.139**	**2.977**	**3.069**
	4,57 − 7,73	1.641	1.652	2.087	2.101
	7,73 − 10,9	-0.733	-0.690	0.056	0.206
	10,9–14,06	-0.733	-0.690	0.056	0.206
	14,06–17,23	-0.733	-0.690	0.056	0.206
	> 17,23	-0.733	-0.690	0.056	0.206

Legend: TA = Total Area, PLSA = Plains and Escarpment area, HSA = Highland and Escarpment area, SA = Escarpment area. Negative values indicate a weak relationship between the information value class and the occurrence of landslides. Positive values indicate a strong relationship between the class and the occurrence of landslides. The higher the positive values, the stronger the relationship

between 800 and 1200 m. For the geomorphons, TRI, and TWI, the most significant classes were the same across all modeling domains (Table 4).

4.3 Evaluation of model fit

For each modeling domain, the combinations of two and five variables resulted in 21 models. Combinations of three and four variables resulted in 35 models, seven models with six variables, and a single model with all seven variables.

The results of the ROC AUC indicate better performance for HSA and TA modeling domains, with all the produced models above 0.75 and a mean of over 0.91. The SA (AUC ROC mean equal to 0.84) was the modeling domain with the lowest ROC AUC values (Fig. 5). Usually, the models with fewer variables presented the highest dispersion of ROC AUC values, with higher dispersion for the two-variable models (21 combinations for each modeling domain). Nevertheless, the two-variable combinations did not show any outliers. Also, the lowest ROC AUC values are usually for models with two variables. Still, some combinations can display high values, and combinations with more variables do not necessarily present the highest values of AUC ROC. Table 5 shows, for all modeling domains, the models with the highest and lowest ROC AUC values for each number of variables.

Regarding the ACCIT results, all the models with seven variables displayed values equal to zero, showing that the combination of all the predisposing factors violates the conditional independence assumption and should be rejected (ACCIT < 0.4). The models with four to six variables presented wider distribution and higher dispersion of ACCIT values (Fig. 5). Moreover, considering the number of combinations, there is a tendency for models with fewer variables to display higher values of ACCIT. None of the two- and three-variable models presented ACCIT values lower than 0.6, showing higher independence between the predisposing factors for these models. Also, for all the modeling domains, the models with four variables have more than 75% of the combinations with values higher than 0.5, while for models with six variables, all the results of ACCIT are lower than 0.3.

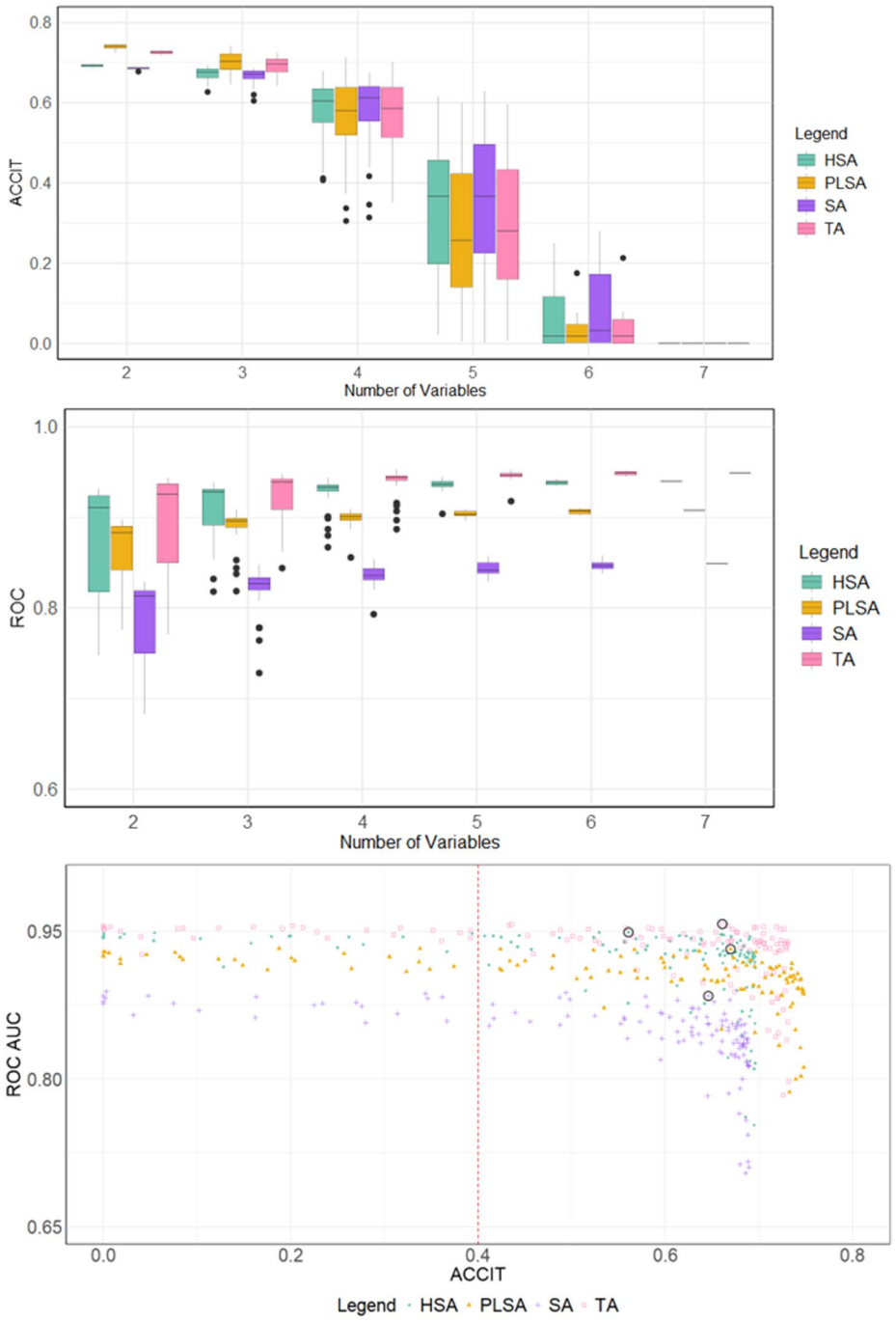

Fig. 5 (**a**) ROC AUC values and number of variables; (**b**) ACCIT results and number of variables; (**c**) Selected models (circled in black) according to ACCIT and ROC AUC values. The red line corresponds to the threshold of acceptable conditional independence among the predisposing factors

Table 5 Landslide susceptibility models with the lowest and highest ROC AUC value for each modeling domain, according to the number of predisposing factors. Best performing models are highlighted in bold type

Model	*N*. of factors	Landslide predisposing factors	ACCIT	ROC AUC
TA 1	7	Aspect, Curvature, Elevation, Geomorphons, Slope, TRI, TWI	0.000	0.954
TA 2	6	Aspect, Curvature, Elevation, Geomorphons, Slope, TRI	0.000	0.956
TA 8	6	Curvature, Elevation, Geomorphons, Slope, TRI, TWI	0.040	0.945
TA 9	5	Aspect, Elevation, Geomorphons, Slope, TRI	0.433	0.956
TA 29	5	Aspect, Curvature, Elevation, Geomorphons, TWI	0.041	0.927
TA 30	**4**	**Aspect**, **Elevation**, **Geomorphons**, **TRI**	**0.661**	**0.957**
TA 64	4	Aspect, Curvature, Geomorphons, TWI	0.640	0.897
TA 65	3	Aspect, Geomorphons, Slope	0.667	0.955
TA 99	3	Aspect, Curvature, TWI	0.710	0.850
TA 100	2	Aspect, Slope	0.727	0.953
TA 120		Aspect, Curvature	0.726	0.784
HSA 1	7	Aspect, Curvature, Elevation, Geomorphons, Slope, TRI, TWI	0.000	0.945
HSA 2	6	Aspect, Curvature, Elevation, Geomorphons, Slope, TRI	0.000	0.948
HSA 8	6	Curvature, Elevation, Geomorphons, Slope, TRI, TWI	0.250	0.933
HSA 9	5	Aspect, Curvature, Elevation, Geomorphons, TRI	0.055	0.949
HSA 29	5	Aspect, Curvature, Elevation, Geomorphons, TWI	0.128	0.914
HSA 30	**4**	**Aspect**, **Elevation**, **Geomorphons**, **TRI**	**0.561**	**0.949**
HSA 64	4	Aspect, Curvature, Geomorphons, TWI	0.560	0.877
HSA 65	3	Aspect, Elevation, Slope	0.659	0.947
HSA 99	3	Aspect, Curvature, TWI	0.667	0.822
HSA 100	2	Aspect, Slope	0.691	0.945
HSA 120	2	Curvature, TWI	0.695	0.753
PLSA 1	7	Aspect, Curvature, Elevation, Geomorphons, Slope, TRI, TWI	0.000	0.925
PLSA 2	6	Aspect, Curvature, Elevation, Geomorphons, Slope, TWI	0.000	0.929
PLSA 8	6	Curvature, Elevation, Geomorphons, Slope, TRI, TWI	0.175	0.911
PLSA 9	5	Aspect, Elevation, Geomorphons, Slope, TWI	0.188	0.933
PLSA 29	5	Curvature, Elevation, Slope, TRI, TWI	0.506	0.902
PLSA 30	4	Aspect, Elevation, Geomorphons, Slope	0.424	0.932
PLSA 64	4	Aspect, Curvature, Geomorphons, TWI	0.535	0.872
PLSA 65	**3**	**Aspect**, **Geomorphons**, **Slope**	**0.670**	**0.932**
PLSA 99	3	Curvature, Geomorphons, TWI	0.722	0.834
PLSA 100	2	Aspect, Slope	0.735	0.917
PLSA 120	2	Aspect, Curvature	0.733	0.787
SA 1	7	Aspect, Curvature, Elevation, Geomorphons, Slope, TRI, TWI	0.000	0.879
SA 2	6	Aspect, Curvature, Elevation, Geomorphons, TRI, TWI	0.003	0.889
SA 8	6	Curvature, Elevation, Geomorphons, Slope, TRI, TWI	0.280	0.857
SA 9	5	Aspect, Elevation, Geomorphons, TRI, TWI	0.494	0.888
SA 29	5	Curvature, Elevation, Slope, TRI, TWI	0.560	0.841
SA 30	**4**	**Aspect**, **Geomorphons**, **TRI**, **TWI**	**0.646**	**0.884**
SA 64	4	Aspect, Curvature, Geomorphons, TWI	0.595	0.820
SA 65	3	Aspect, Geomorphons, TRI	0.669	0.880
SA 99	3	Curvature, Geomorphons, TWI	0.679	0.765
SA 100	2	Aspect, TRI	0.685	0.856
SA 120	2	Curvature, Geomorphons	0.686	0.705

Considering the number of variables, the ACCIT and ROC AUC results, four different models were selected, one for each modeling domain (Fig. 5). The TA30 was selected as the best model for the TA domain. This model was created with four variables (aspect, elevation, geomorphons, and TRI), presenting an ACCIT value of 0.661 and ROC AUC of 0.957. The same set of variables was chosen as the best model for the HSA domain (HSA30), however, the ACCIT and ROC AUC values were slightly lower than for the TA domain (respectively, 0.561 and 0.949). For the PLSA domain, the selected model (PLSA65) was composed of only three variables (aspect, geomorphons, and slope), displaying ACCIT equal to 0.670 and a ROC AUC value of 0.932. In the case of the SA domain, the model SA30 was selected, presenting ACCIT and ROC AUC values, respectively, of 0.646 and 0.884. This model was generated by the combination of aspect, geomorphons, TRI, and TWI.

All the selected models displayed reasonable predictive capacities, with the highest values for **TA30** and the lowest for **SA30** (Fig. 6). The AUC of prediction rate curves for the selected models of TA, HSA, PLSA, and SA are, respectively, 0.938, 0.924, 0.920, and 0.868. Through visual inspection, it is possible to note some major changes in the classification of the escarpment slopes (represented in all models) (Fig. 7). In this compartment, the TA30, HSA30, and PLSA65 models presented a greater generalization of the most susceptible areas, whereas the SA30 model provided a better depiction of these areas.

To produce the final susceptibility map for the GCCS, we merged the HSA30, PLSA65, and SA30 models, already classified into five classes (Very Low, Low, Moderate, High, and Very High), excluding the escarpment area of HSA30 and PLSA65. In this way, the final map of the geopark presents the highland modeled through HSA30; the plain through

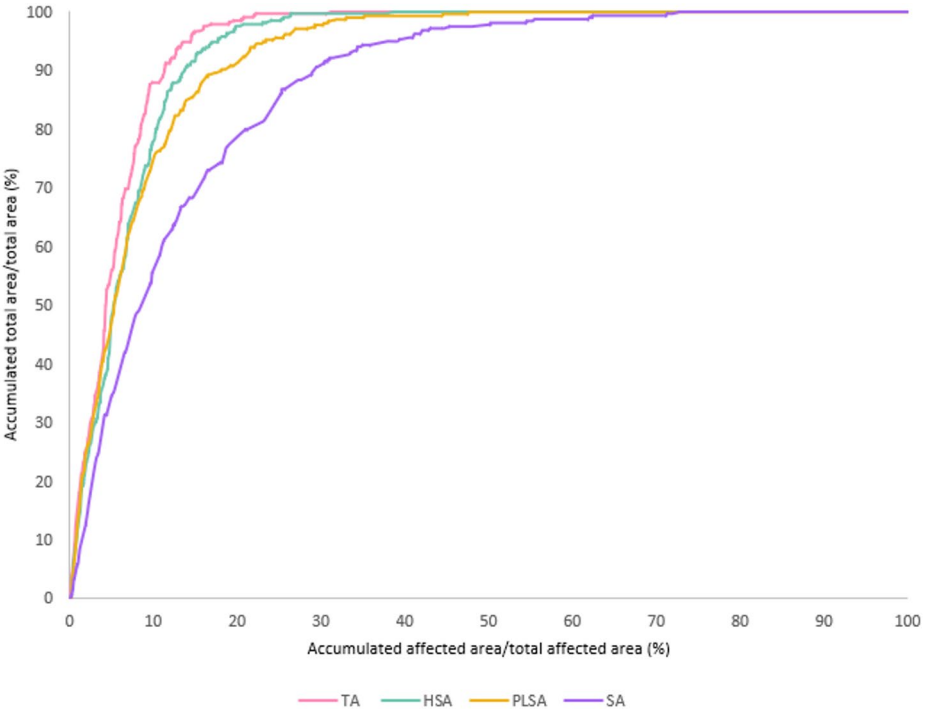

Fig. 6 Prediction curve of the selected models

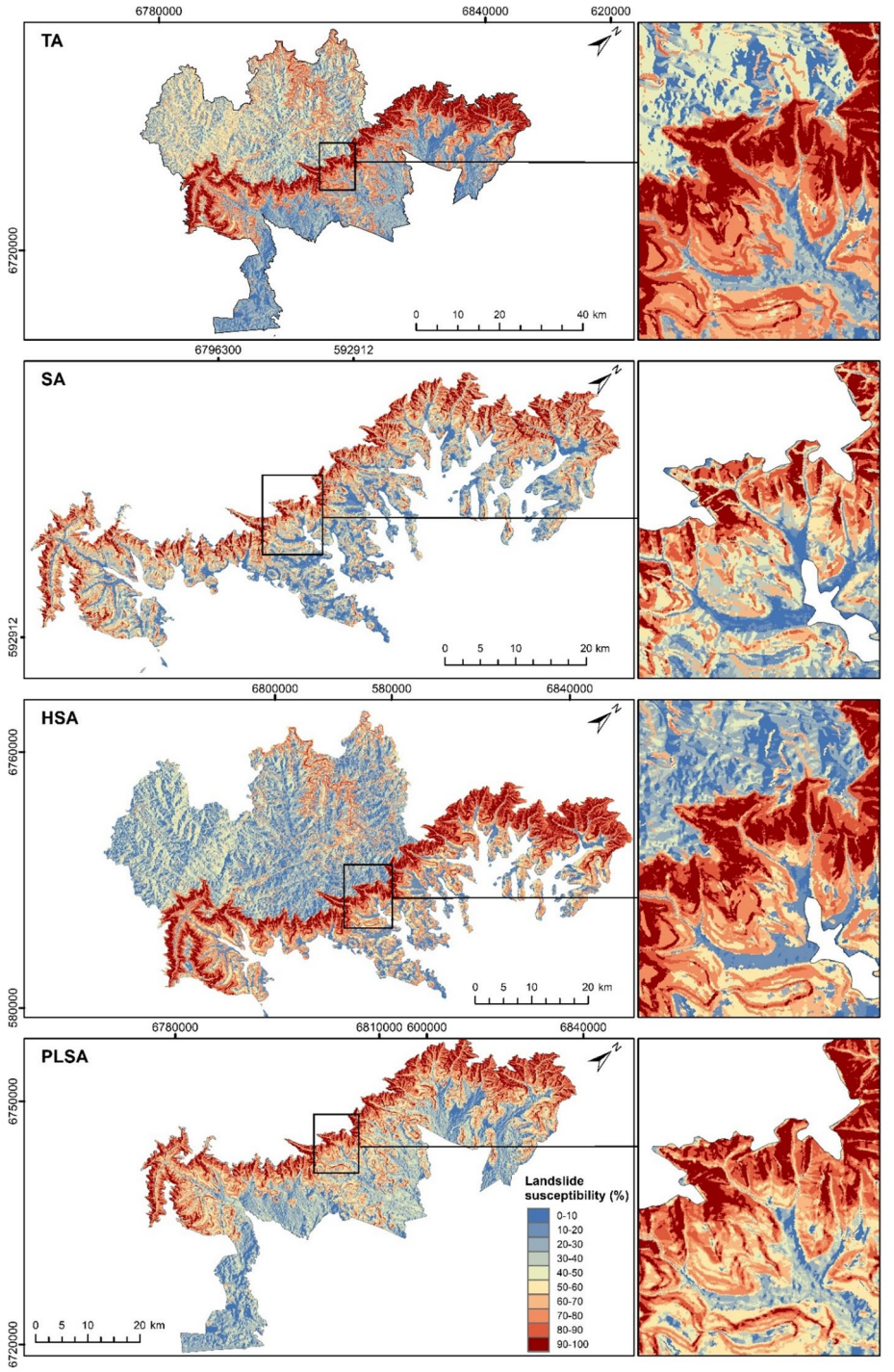

Fig. 7 Selected models classified into ten landslide susceptibility classes

PLSA65; and the escarpment through SA30 (Fig. 8). The final map of the GCCS displays 59,5% of Very Low susceptible area, 19,7% of Low, 12,1% of Moderate, 5,4% of High, and 3,3% of Very High. Additionally, many geosites are located in areas classified as Very High (geosites 8 and 19), High (geosite 9), and Moderate (geosites 2, 3, 12, 15, 16, 20, and 27) (Fig. 8).

5 Discussion

5.1 Landslide inventories

The landslide inventories displayed considerably high overall accuracies (all above 0.85), indicating that both the segmentation tuning and the definition of the classification rules were effective. The accuracy difference between Inventory I (derived from SPOT-3 imagery) and the other two inventories (derived from RapidEye imagery) is noteworthy. We attribute this difference to the different spatial resolutions of the datasets used (10 m and 5 m, respectively). Among the two inventories produced with RapidEye imagery, there is a slight difference in the accuracy, which can be related to the total landslide-affected area in Inventories II and III (0.37 km² and 1.48 km², respectively) and differences in the characteristics of the event. Inventory II contains a significant number of affected areas related to shallow landslides, elongated and with reduced width, that are highlighted in previous studies as difficult to detect (Amatya et al. 2021; Bonini et al. 2022). On the other hand, Inventory III contains mostly affected areas related to debris flows and other hydrodynamic

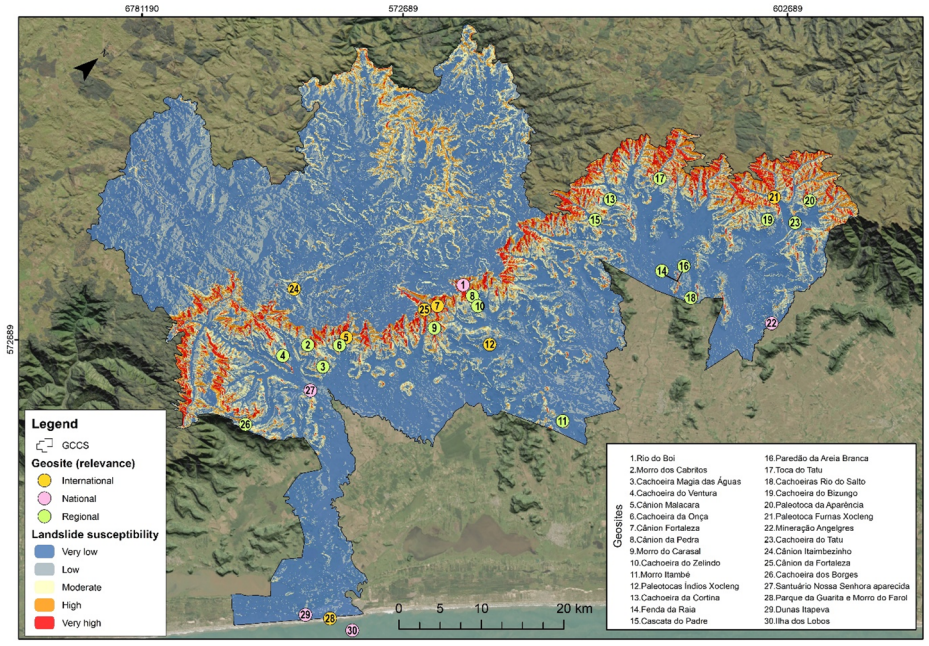

Fig. 8 Final landslide susceptibility map and location of geosites

processes, which display a consistent spectral behavior and geometry (occupying the valley bottom in a more or less continuous manner).

Regardless of the preference in the literature for the use of temporal partition in the case of multi-temporal inventories (Zêzere et al. 2017) there was a significant disparity between the number of landslide initiation points contained in Inventory I and its counterparts: summed, Inventory II and Inventory III have 162 initiation points within the boundaries of the GCCS, while for Inventory I have 505 initiation points. Therefore, we opted for a random spatial partition instead of a temporal one, since the discrepancy in the number of landslides triggered in each of the generalized events could provide misleading results due to the imbalance between training and test subsets if a temporal partition criterion were employed.

Also, considering the distinct characteristics of the mapped landslide events and the images' spatial resolutions, we considered initiation points more suitable than the whole landslide scar area. This is due to the fact that in the 1995 event (the one with the largest landslide-affected area), the landslide scars, in some cases, covered almost the entire slope, and the SPOT HRV image (10 m resolution) did not allow the correct separation between initiation and transport areas. Including transport and deposition areas in the susceptibility modeling could produce inaccuracies in the final maps once the influence of some classes of predisposing factors is overrated, as well as the high susceptibility areas in the territory (Petschko et al. 2014). On the other hand, the number of initiation points is underestimated for the 1995 event since many coalescent scars may contain more than one rupture zone. However, once more, image resolution was an obstacle when trying to detect and individualize landslides (Fig. 9).

The existence of protected areas and the steeper terrains of the escarpment impose some obstacles to the occupation of the slopes. In that way, the greater population density within the GCCS is concentrated in the plains, in some cases distant from the escarpment. Therefore, many landslide events are not reported, or when they are, they are misclassified as floods or flash floods due to changes in the process dynamics along their path and when they reach urban agglomerations. This is a common situation in sparsely occupied areas since the official reporting of landslides is mainly done when damage occurs. (Steger et al. 2021). Additionally, the absence of high temporal resolution imagery for the territory in the early 2000s makes it difficult to ascertain some events' precise date of occurrence (Inventory II and Inventory III).

The 1995 event was triggered by an exceptional weather phenomenon during which cumulonimbus clouds were observed with a basal height of around 500 m, shifting towards the slopes of the Serra Geral and creating persistent orographic rainfall on the headwaters (Pellerin et al. 1997). Usually, in the south of Brazil, these clouds have a basal height above 1.000 m (Pellerin et al. 1997). Although the official records of this event indicate an estimate between 206 and 225 mm of rainfall, the weather station that provided the forecast was located more than 150 km from the affected area. In that way, there is no realistic estimate of the rainfall that triggered the 1995 event, as well as for the other events (Inventories II and III), whose precise date of occurrence is uncertain. Even if we could precisely ascertain the date of the two other events, the spatial density of the weather stations in the region and the absence of stations in the escarpment hinder the identification of the rainfall volume that triggered the events.

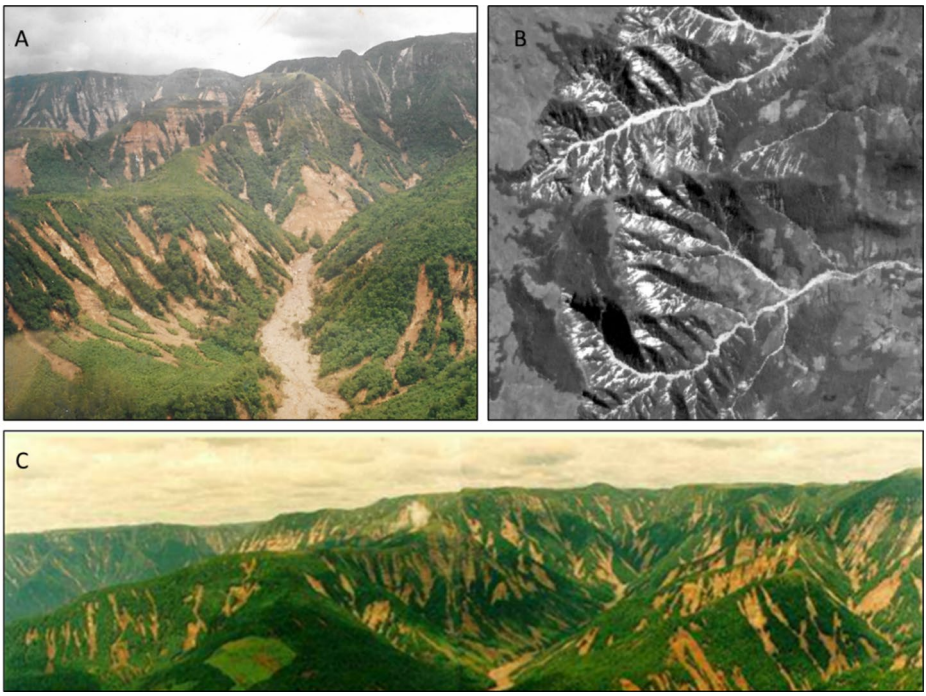

Fig. 9 (**a**, **c**) 1995 event in Jacinto Machado and Timbé do Sul municipality. It is possible to note that many landslides occurred close to the watershed divides. (**b**) SPOT image resolution makes it difficult to differentiate rupture, transport, and deposition zones of coalescent scars. Source: (**a**, **c**) Joel Pellerin

5.2 Susceptibility assessment

The analysis of predisposing factors and their classes IVs highlights some important information about the relief controls over landslides in the GCCS. The slope angle is one of the most frequently selected inputs for statistically-based models (Reichenbach et al. 2018). For all the modeling domains, the slope angle class above 25° displayed some explanatory power of the landslide distribution (IV > 1.0), particularly for the class above 45°. However, although the slope angle can be an important predisposing factor of landslides, in its simple form, it may not be able to capture the influence of slope gradient changes on slope stability in complex relief areas. In our case, the terrain ruggedness index (TRI) was more important in constructing the best models and showed less dependence on other parameters. In that way, only the PLSA65 was built with the slope angle among its predisposing factors. For all the other domains, the slope angle was not used in the selected models; instead, the TRI was used. The TRI provides information on local surface variability, which is an average of slope-adjacent neighbors. (Riley et al. 1999; Trevisani et al. 2023). The values of TRI are expected to be higher in unstable areas. They can be more effectively related to landslide distribution than simple metrics (i.e., slope and mean slope), especially for large failures (Reichenbach et al. 2018). Therefore, the TRI class above 9.24 displayed the highest IV for the selected models.

However, it is important to note that the classes of the predisposing factors with the highest IVs do not necessarily correspond to the class where most landslides occur. The IV results from the relation of the affected area in a class of the predisposing factor to the total area of this same class. This can be verified through the difference in the classes with higher IVs of the same predisposing factor across different modeling domains. For elevation, TA and HSA modeling domains presented the highest IV for classes between 600 and 800 m, while for PLSA and SA, these values were higher (above 800 m for PLSA and 1000 m for SA). TA and HSA encompass the highland areas usually located above 1000 m. Thus, there is a larger area above this elevation threshold in these modeling domains; in this way, the IV is smaller for this class in TA and HSA. The elevation parameter was used only to compute TA30 and HSA30 models.

The aspect and geomorphons predisposing factors are present in all the selected models (Table 5). There is no consensus in the literature about the influence of aspect in landslide occurrence and distribution, although for some authors, the aspect can be considered one of the most important predisposing factors (Galli et al. 2008; Lee 2005), and in statistically-based methods, it is the second most frequently used parameter (Reichenbach et al. 2018; Dias et al. 2021b). Previous research about the influence of aspect in statistical methods by Capitani et al. (2013) identified that aspect can significantly influence landslide distribution, especially for shallow landslides (superficial). As a simple morphometric variable, the aspect may be controlled by the influence of local conditions (Reichenbach et al. 2018). Considering the characteristics of GCCS territory, presenting many features, especially on the basaltic rocks, the aspect may act as a proxy variable related to structural controls over the slope's geometric properties, such as the strata dip angle (Messenzehl et al. 2017; Zêzere et al. 2017).

For our area, the spurs were the geomorphons with the highest IV, followed by slope, hollow, and ridge. The classification shows that the flat, summit, footslope, valley, and depression landforms do not influence the landslide distribution. Spurs can display high slope angles, slopes, and ridges. Also, in the three mapped events, most of the landslide initiation points are located close to the watershed divides, a piece of information that can explain the higher IVs assumed by the abovementioned geomorphons. However, in the case of the hollows, there is also a relationship between slope and curvature that implies flow convergence and, consequently, an enhanced predisposition to shallow landslides and debris flows (e.g., Zhang et al. 2020). The geomorphons are not commonly used in susceptibility studies, but some authors have found good results when relating geomorphons and landslide distribution (Steger et al. 2021; Acosta-Quesada and Quesada-Román 2024). Geomorphons, as complex variables, can better explain the variability of terrain characteristics and perform better than basic variables (e.g., curvature). The curvature is the only predisposing factor that is not present in any of the selected models. However, this variable is highlighted as one of the most important for many studies conducted in Brazil (Fernandes et al. 2004; Vieira et al. 2018; Dias et al. 2021a; Bonini et al. 2022).

Among these more complex variables, the TWI class under 4.57 displayed high values for all the domains; however, this predisposing factor is present only in the SA30 model. This can be related to the fact that for the other modeling domains, the presence of classes with higher TWI is widespread compared to the escarpment area. The TWI is a variable that can indicate areas of potential water flow accumulation, often waterlogged (Moore et al. 1991; Różycka et al. 2017). In that way, lower values of TWI can be related to small

specific contribution areas, which favor rapid saturation during rainfall and are most often affected by landslides.

We assume that ACCIT proved to be an effective tool for analyzing the independence among the predisposing factors and the variables' influence in the different modeling domains. Although information value studies have been widely carried out in the last decades, it is not common to assess the independence of predisposing factors, which is an assumption of the bivariate methods (Pereira et al. 2012). In Brazil, few studies have carried out a conditional independence diagnosis (e.g., Araújo et al. 2021). The presence of conditional dependence among the independent variables does result in some overestimation of spatial probability (Agterberg and Cheng 2002), and we argue that future studies should include this type of test in their modeling protocols.

The adopted strategy, to model heterogeneous domains, proved to be effective for our study area, since we could realize that the selected predisposing factors behaved differently for each domain. In that way, not only do the selected models have different combinations, but also it is possible to notice that some classes of variables can better explain how the predisposing factors were selected in the respective domain. Petschko et al. (2014) found similar results by modeling geological domains separately, although, for our area, it was not possible to model the domains without the escarpment area. Moreover, previous studies in GCCS territory have already demonstrated that the analysis of mass movement susceptibility should be carried out considering the different characteristics of the geomorphological compartment, even for qualitative assessments (Sugiyama and Gomes 2023).

A careful interpretation of the landscape can exemplify the reasons for adopting different modeling domains (Fig. 10). In the GCCS territory, the highlands are mainly formed by elevated and flat areas, except for the valleys carved by the drainage that mostly display structural controls. In the same way, the plains areas present gentle slopes (usually less than 5°), and most existing rivers are typical of low-energy areas, forming extensive flood plains. In contrast with these flat areas, the escarpment presents highly steep slopes, in many cases

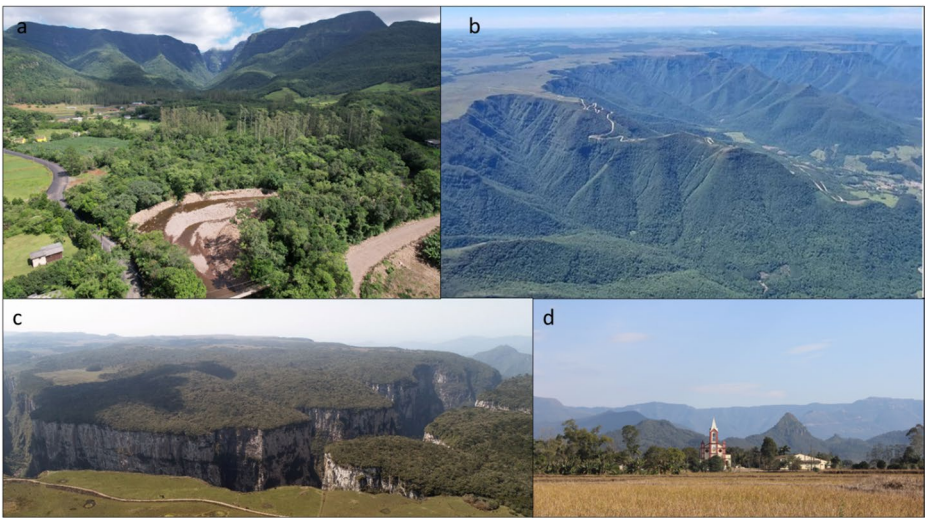

Fig. 10 (**a**, **b**) The landscape of GCCS is marked by the contrast between the steeper slopes of the escarpment (**c**) and the flat areas of the highlands **(**d) and plains. Source: (**b**) Fernando Daminani

Fig. 11 (**a**) Planet Scope Image (14/11/2024) of the area affected by the 2024 event. The image highlights the affected areas and older scars from the 1995 event. (**b**) The 22 landslide-affected areas are classified as moderately to very susceptible. (**c**) Most of the shallow landslides occurred near the headwaters, characterized by thin, elongated features. (**d**) At least six debris flows were triggered by this event, impacting a large area of the plains

controlled by fractures and joints, where it is also possible to find canyons and waterfalls. This abrupt contrast between these areas results in different amounts of sediments available, energy (erosion power), and characteristics of the geomorphological process. Thus, it is not unexpected that landslide predisposing factors behave differently in each geomorphological compartment.

We assume that the final map obtained by merging the different domains is a satisfactory depiction of landslide susceptibility in the area, especially considering the characteristics of GCCS territory. Moreover, since the escarpment area was modeled separately, it is possible to differentiate the very susceptible areas, which for other of the produced models could be almost the whole escarpment. Thinking in Geopark management, this is a relevant achievement to help select the most critical areas to assess the hazard and create risk prevention and mitigation plans. Indeed, many geosites are located in moderately to very high susceptible areas or adjacent areas, which can be in the transport or deposition zones (Fig. 8).

On November 6, 2024, another landslide event occurred in the Serra Geral escarpment, in one of the watersheds affected by the 1995 event (Fig. 11). This event happened after the compilation of our landslide inventories and, therefore, these landslides were not included in the modeling steps. However, a quick assessment of the affected areas revealed that all the landslides occurred in areas classified as moderate to very high susceptibility in our map. Of the 23 landslides triggered, 14 were in areas classified as having very high susceptibility, seven in high susceptibility, and two in a moderate susceptibility area. It is important to note that many landslides triggered near watershed divides are placed close to the boundaries

between different susceptibility classes. This may be related to the DEM resolution, which can influence the detailing of the susceptibility classification. Given that the 2024 landslides were not considered during model construction, the location of the majority of affected areas in the very high and high susceptibility classes supports the considerably high predictive capacity of the final models.

Four limitations of this study can be indicated: (1) there is some degree of subjectivity in the landslide affected-areas detection strategy, since the rules are defined by the user and they tend to be both site- and event-specific (i.e., the same set of rules may not perform well for different areas and/or landslide events); (2) the best DEM was available at medium spatial resolution and this affects both the differentiation between landslides and hydrodynamic processes and the detailing of the susceptibility assessment; (3) as is the case with most global statistical models, the use of single weighting factors for the independent variables can be problematic in areas with complex geomorphological setting, and also some of the independent variables may have non-linear relationships with the dependent one that are not captured by the models; and (4) in the majority of the generalized events that occurred in our area the landslides on the slopes tend to trigger debris flows with long runouts, that remobilize the valley bottom materials and reach exposed elements far from the point where the shallow landslides were initiated (e.g., built infrastructure).

Concerning the first one, we consider it a minor problem for our approach, given that the majority of landslide inventories in Brazil are produced by conventional visual interpretation, whose procedures may be less systematic than the ones employed in this study. About the second limitation, this data type is unavailable in most of Brazil in high resolution, like LiDAR Digital Terrain Models with wide territorial coverage. The third limitation is common to our study and the ones that employed global multivariate methods, such as logistic regression. It was mitigated by the use of heterogeneous modeling domains, allowing different combinations of predisposing factors and weighting factors for each geomorphological compartment. Finally, the fourth and last limitation can be overcome in future studies that will strongly benefit from this work's products to perform debris flow susceptibility and trajectory analysis (which was out of scope here).

6 Conclusions

This research produced inventories for three generalized mass movement events that occurred in the last 30 years in the Caminhos dos Cânions do Sul UNESCO Geopark (GCCS), using a semi-automatic Object-Based Image Analysis (OBIA) procedure. The events were identified in archive orbital images from 1996, 2009, and 2011. The results show that an area of 12,2 km² was affected by debris flows and other hydrodynamic processes, and 7,13 km² by shallow landslides. Afterwards, a shallow landslide statistically based susceptibility assessment was conducted for four different modeling domains based on the geomorphological compartments (total area, highland, escarpment, and plains). Seven different predisposing factors were combined, resulting in 120 combinations for each modeling domain. The results show a better response of aspect and geomorphons (present in all four selected models), and for composite morphometric variables such as the TWI and the TRI.

The modeling strategy based on heterogeneous domains proved to be efficient in analyzing different controls exerted by the predisposing factor classes in each geomorphological

compartment. Additionally, this strategy, combined with the conditional independence test, prevented a generalization of the very high susceptibility class and provided a robust modeling framework. The final map, composed by the combination of the three modeling domains corresponding to the geomorphological compartments, resulted in 59,5% of Very Low susceptibility area, 19,7% of Low, 12,1% of Moderate, 5,4% of High, and 3,3% of Very High.

Limitations due to data resolution (satellite imagery and DEM), the occurrence of cascading landslides and hydrodynamic processes, and nonlinear relationships between dependent and independent variables were identified and acknowledged.

Nonetheless, while acknowledging the study's limitations, the final susceptibility map yielded satisfactory results, enabling the identification of 10 geosites predominantly situated within landslide-prone areas. These findings are expected to make substantial contributions to the development and implementation of geohazard risk prevention, mitigation, and management plans. Those plans can support the safeguarding of the GCCS geoheritage and the tourists, and are especially urgent due to the expected changes in landslide frequency and magnitude related to changes in rainfall patterns that are expected as a consequence of global climate change.

Therefore, the results presented in this paper can be useful for future studies to determine the temporal probability of landslides in the Geopark area. Since the weather station distribution does not allow a feasible estimation of rainfall thresholds, this could be carried out by testing the most suitable rainfall measures from spaceborne sensors. This analysis could then support a spatially explicit hazard assessment capable of simulating runout areas and potential infrastructural and geoheritage impacts related to landslide occurrence.

Acknowledgements We are thankful to the Graduate Programme in Physical Geography of the University of São Paulo. We are also thankful for the valuable comments provided by the two anonymous reviewers, wich significantly improved our paper, and the Editor's careful handling of the manuscript.

Author contributions All authors contributed to the study conception and design. Material preparation, data collection and analysis were performed by Marina Tamaki de Olveira Sugiyama, and José Eduardo Bonini. The first draft of the manuscript was written by Marina Tamaki de Oliveira Sugiyama and José Eduardo Bonini, and all authors commented on previous versions of the manuscript. All authors read and approved the final manuscript.

Funding This research was funded by the São Paulo Research Foundation (FAPESP) in the frame of the grant #2021/04621-6, grant #2022/09132-6, and grant #2023/16080-5.

Declarations

Competing interests The authors have no relevant financial or non-financial interests to disclose.

References

Acosta-Quesada M, Quesada-Román A (2024) Landslides and flood hazard mapping using Geomorphological methods in Santa ana, Costa Rica. Int J Disaster Risk Reduct 113:104882. https://doi.org/10.1016/j.ijdrr.2024.104882

Adams R, Bischof L (1994) Seeded region growing. IEEE Trans Pattern Anal Mach Intell 16:641–647. https://doi.org/10.1109/34.295913

Agterberg FP, Cheng Q (2002) Conditional independence test for Weights-of-Evidence modeling. Nat Resour Res 11:249–255

Aleotti P, Chowdhury R (1999) Landslide hazard assessment: summary review and new perspectives. Bull Eng Geol Environ 58:2144. https://doi.org/10.1007/s100640050066
Amatya P, Kirschbaum D, Stanley T, Tanyas H (2021) Landslide mapping using object-based image analysis and open source tools. Eng Geol 282:106000. https://doi.org/10.1016/j.enggeo.2021.106000
Amatya P, Kirschbaum D, Stanley T (2022) Rainfall-induced landslide inventories for lower Mekong based on planet imagery and a semi-automatic mapping method. Geosci Data J 9:315–327. https://doi.org/10.1002/gdj3.145
Araújo JP, de Barella C, Fernandes CF NF (2021) Modelling landslide susceptibility using the weight of evidence method in a tropical mountains region. Geosciences 40:137–155. https://doi.org/10.5016/GEOCIENCIAS.V40I1.14992
Ardizzone F, Cardinali M, Carrara A et al (2002) Impact of mapping errors on the reliability of landslide hazard maps. Nat Hazards Earth Syst Sci 2:314. https://doi.org/10.5194/nhess-2-3-2002
Beven KJ, Kirby MJ (1979) A physically based, variable contributing area model of basin hydrology. Hydrol Sci Bull 24:43–69
Bierman P, Montgomery D (2019) Key concepts in geomorphology, 2nd edn. W. H. Freeman
Blahut J, van Westen CJ, Sterlacchini S (2010) Analysis of landslide inventories for accurate prediction of debris-flow source areas. Geomorphology 119:36–51. https://doi.org/10.1016/j.geomorph.2010.02.017
Bonham-Carter GF (1994) Geographic Information Systems for Geoscientists. Elsevier. https://doi.org/10.1016/C2013-0-03864-9
Bonham-Carter GF, Agterberg FP, Wright DF (1989) Weights of evidence modelling: a new approach to mapping mineral potential. In: Agterberg FP, Boham-Carter GF (eds) Statistical applications in Earth sciences. Geological Survey of Canada, Ottawa, pp 171–183
Bonini JE, Vieira BC, Martins TD (2022) Semiautomatic inventory and Geomorphological characterization of mass movements using high-resolution images and open-source software in the Ribeira de Iguape valley, Brazil. J South Am Earth Sci 119. https://doi.org/10.1016/j.jsames.2022.104029
Bordoni M, Galanti Y, Bartelletti C et al (2020) The influence of the inventory on the determination of the rainfall-induced shallow landslides susceptibility using generalized additive models. Catena (Amst) 193:104630. https://doi.org/10.1016/j.catena.2020.104630
Brabb E (1984) Innovative Approaches for Landslide Hazard Evaluation. In: IV International Symposium on Landslides. Toronto, pp 307–323
Bradley AP (1997) The use of the area under the ROC curve in the evaluation of machine learning algorithms. Pattern Recognit 30:1145–1159. https://doi.org/10.1016/S0031-3203(96)00142-2
Brilha J (2018) Geoheritage and geoparks. Geoheritage: Assess Prot Manage 323–335. https://doi.org/10.1016/B978-0-12-809531-7.00018-6
Bucci F, Santangelo M, Fiorucci F et al (2021) Geomorphologic landslide inventory by air photo interpretation of the high Agri Valley (Southern Italy). J Maps 17:376–388. https://doi.org/10.1080/17445647.2021.1943552
Capitani M, Ribolini A, Bini M (2013) The slope aspect: A predisposing factor for landsliding? Comptes Rendus Géoscience 345:427–438. https://doi.org/10.1016/j.crte.2013.11.002
Chung CF, Fabbri AG (1999) Probabilistic prediction models for landslide hazard mapping. Photogramm Eng Remote Sens 65:1389–1399
Chung CF, Fabbri AG (2003) Validation of Spatial prediction models for landslide hazard mapping. Nat Hazards 30:451–472. https://doi.org/10.1023/B:NHAZ.0000007172.62651.2b
Conrad O, Bechtel B, Bock M et al (2015) System for automated geoscientific analyses (SAGA) v. 2.1.4. Geosci Model Dev 8:1991–2007. https://doi.org/10.5194/gmd-8-1991-2015
Corominas J, van Westen C, Frattini P et al (2014) Recommendations for the quantitative analysis of landslide risk. Bull Eng Geol Environ 73:209–263. https://doi.org/10.1007/s10064-013-0538-8
Dias HC, Gramani MF, Grohmann CH et al (2021a) Statistical-based shallow landslide susceptibility assessment for a tropical environment: a case study in the southeastern Brazilian Coast. Nat Hazards 108:205–223. https://doi.org/10.1007/S11069-021-04676-Y/FIGURES/9
Dias HC, Hölbling D, Grohmann CH (2021b) Landslide susceptibility mapping in brazil: A review. Geosci (Basel) 11:425. https://doi.org/10.3390/geosciences11100425
Dierickx F, Pavlova I, Gaines S (2016) Natural hazards in UNESCO global geoparks. Eur Geoparks Magazine 13:16–17
Dietrich WE, Montgomery DR (1998) Shalstab: A Digital Terrain Model for Mapping Shallow Landslide Potential. Technical Report, National Council for Air and Stream Improvement
Dikau R, Cavallin A, Jäger S (1996) Databases and GIS for landslide research in Europe. Geomorphology 15:227–239. https://doi.org/10.1016/0169-555X(95)00072-D
EGN – European Geoparks Network (2012) 5th International UNESCO Conference on Geoparks – Shimabara Declaration5th International UNESCO Conference on Geoparks – Shimabara Declaration. Global Geoparks Network. https://www.europeangeoparks.org/?p=1974

Fassoulas C et al (2018) UNESCO Global Geoparks: living laboratories to mitigate natural induced disasters and strengthen communities' resilience. In: Antronico, L. & Marincioni, F. (Eds.) Natural Hazards and Disaster Risk Reduction Policies, pp.175–197

Fawcett T (2006) An introduction to ROC analysis. Pattern Recognit Lett 27:861–874. https://doi.org/10.1016/j.patrec.2005.10.010

Fernandes NF, Guimarães RF, Gomes RAT et al (2004) Topographic controls of landslides in Rio de janeiro: field evidence and modeling. In: Catena. Elsevier, pp 163–181

Franck AG, Kobiyama M (2024) Investigation and mapping of natural hazards areas related to mass movements in a geopark, in Southern Brazil. J S Am Earth Sci 141:104926. https://doi.org/10.1016/j.jsames.2024.104926

Fratini P, Crosta G, Carrara A (2010) Techniques for evaluating the performance of landslide susceptibility models. Eng Geol 11:62–72. https://doi.org/10.1016/j.enggeo.2009.12.004

Fressard M, Thiery Y, Maquaire O (2014) Which data for quantitative landslide susceptibility mapping at operational scale? Case study of the pays d'auge plateau hillslopes (Normandy, France). Nat Hazards Earth Syst Sci 14:569–588. https://doi.org/10.5194/nhess-14-569-2014

Fukuoka H (2014) Landslides, geoparks and world heritage. Science reports of Nigata (Geology)

Galli M, Ardizzone F, Cardinali M et al (2008) Comparing landslide inventory maps. Geomorphology 94:268–289. https://doi.org/10.1016/J.GEOMORPH.2006.09.023

Guzzetti F, Carrara A, Cardinali M, Reichenbach P (1999) Landslide hazard evaluation: a review of current techniques and their application in a multi-scale study. Cent Italy Geomorphology 31:181–216. https://doi.org/10.1016/S0169-555X(99)00078-1

Hawker L, Uhe P, Paulo L et al (2022) A 30 m global map of elevation with forests and buildings removed. Environ Res Lett 17:024016. https://doi.org/10.1088/1748-9326/ac4d4f

IBGE – Instituto Brasileiro de Geografia e Estatística (2018) Geomorfologia 1:250.000. Banco de Dados e Informações Ambientais. https://bdiaweb.ibge.gov.br/#/home

IBGE – Instituto Brasileiro de Geografia e Estatística (2009) Manual técnico de geomorfologia. Rio de Janeiro

Carta de suscetibilidade a movimentos gravitacionais de massa e inundações: município de Timbé do Sul – SC. IPT – Instituto de Pesquisas Tecnológicas, Rigeo (2015a) https://rigeo.sgb.gov.br/handle/doc/15156

Carta de suscetibilidade a movimentos gravitacionais de massa e inundações: município de Timbé do Sul – SC. IPT – Instituto de Pesquisas Tecnológicas, Rigeo (2015b) https://rigeo.sgb.gov.br/handle/doc/15156

Jones C (2008) History of geoparks. Geol Soc Lond Special Publications 300:273–277. https://doi.org/10.1144/SP300.21

Lacerda WA (2007) Landslide initiation in saprolite and colluvium in Southern brazil: field and laboratory observations. Geomorphology 87:104–119. https://doi.org/10.1016/j.geomorph.2006.03.037

Lacroix P, Zavala B, Berthier E, Audin L (2013) Supervised method of landslide inventory using panchromatic SPOT5 images and application to the Earthquake-Triggered landslides of Pisco (Peru, 2007, Mw8.0). Remote Sens (Basel) 5:2590–2616. https://doi.org/10.3390/rs5062590

Lee S (2005) Application of logistic regression model and its validation for landslide susceptibility mapping using GIS and remote sensing data. Int J Remote Sens 26:1477–1491. https://doi.org/10.1080/01431160412331331012

Lee Y, Jayakumar R (2021) Economic impact of UNESCO global geoparks on local communities: comparative analysis of three UNESCO global geoparks in Asia. Int J Geoheritage Parks 9:189–198. https://doi.org/10.1016/j.ijgeop.2021.02.002

Lee C-T, Huang C-C, Lee J-F et al (2008) Statistical approach to earthquake-induced landslide susceptibility. Eng Geol 100:43–58. https://doi.org/10.1016/j.enggeo.2008.03.004

McColl ST (2015) Landslide causes and triggers. In: Shroder JF, Davies T (eds) Landslide hazards, risks, and disasters. Elsevier, pp 17–42

Meena SR, Ghorbanzadeh O, van Westen CJ et al (2021) Rapid mapping of landslides in the Western Ghats (India) triggered by 2018 extreme monsoon rainfall using a deep learning approach. Landslides 18:1937–1950. https://doi.org/10.1007/s10346-020-01602-4

Messenzehl K, Meyer H, Otto J-C et al (2017) Regional-scale controls on the Spatial activity of rockfalls (Turtmann valley, Swiss Alps) — A multivariate modeling approach. Geomorphology 287:29–45. https://doi.org/10.1016/j.geomorph.2016.01.008

Milani E et al (2007) Bacia do Paraná. Bol De Geociências 15:265–267

Moore ID, Grayson RB, Ladson AR (1991) Digital terrain modelling: A review of hydrological, geomorphological, and biological applications. Hydrol Process 5:3–30. https://doi.org/10.1002/hyp.3360050103

Morino C, Coratza P, Soldati M (2022) Landslides, a key landform in the global geological heritage. Front Earth Sci (Lausanne) 10:864760. https://doi.org/10.3389/FEART.2022.864760/BIBTEX

Paixao MA et al (2021) Occurrence of Multi-Disasters in the Mampituba river basin, Southern brazil, during the COVID-19 pandemic. Int J Eros Control Eng 13:84–92. https://doi.org/10.13101/ijece.13.84

Pavlova I (2019) Disaster risk reduction at UNESCO global geoparks and biosphere reserves. J World Herit Stud 73–77
Pellerin J, Duarte GM, Scheibe LF et al (1997) Timbé do Sul - Jacinto Machado - Avaliação preliminar Da Extensão Da catástrofe de 23–24/12/95. Geosul 12:71–86
Pereira S, Zêzere JL, Bateira C (2012) Technical note: assessing predictive capacity and conditional independence of landslide predisposing factors for shallow landslide susceptibility models. Nat Hazards Earth Syst Sci 12:979–988. https://doi.org/10.5194/nhess-12-979-2012
Petschko H, Bell R, Brenning A, Glade T (2012) Landslide susceptibility modeling with generalized additive models – facing the heterogeneity of large regions. In: Eberhardt E, Froese C, Turner AK, Leroueil S (eds) Landslides and engineered slopes. Protecting Society through Improved Understanding. Taylor & Francis
Petschko H, Brenning A, Bell R et al (2014) Assessing the quality of landslide susceptibility maps - Case study lower Austria. Nat Hazards Earth Syst Sci 14:95–118. https://doi.org/10.5194/NHESS-14-95-2014
Pimenta L, Freitas M, Sung L (2018) Plano integrado e participativo de Gestão de Risco de desastres do território do Projeto geoparque. Caminhos dos Cânions do Sul
Planet Team (2017) Planet Application Program Interface: In Space for Life on Earth. San Francisco, CA. https://api.planet.com
R Core Team (2019) R: A Language and environment for statistical computing. R-Project. https://www.r-project.org/
Reichenbach P, Rossi M, Malamud BD et al (2018) A review of statistically-based landslide susceptibility models. Earth Sci Rev 180:60–91. https://doi.org/10.1016/J.EARSCIREV.2018.03.001
Reynard E (2009) Geomorphosites: definitions and characteristics. In: Reynard E, Coratza P, Regolini-Bissig G (eds) Geomorphosites. Pfeil, Munich
Reynard E, Coratza P (2016) The importance of mountain geomorphosites for environmental education: examples from the Italian dolomites and the Swiss alps. Acta Geogr Slov 56:291–303. https://doi.org/10.3986/AGS.1684
Riley SJ, De Gloria SD, Elliot R (1999) A terrain ruggedness index that quantifies topographic heterogeneity. Intermt J Sci 5:23–27
Różycka M, Migoń P, Michniewicz A (2017) Topographic wetness index and terrain ruggedness index in geomorphic characterisation of landslide terrains, on examples from the sudetes, SW Poland. Z Für Geomorphologie Supplementary Issues 61:61–80. https://doi.org/10.1127/zfg_suppl/2016/0328
Sawatzky DL, Raines GL, Bonham-Carter GF et al (2009) Spatial Data Modeller (SDM): ArcMAP 9.3 geoprocessing tools for spatial data modeling using weights of evidence, logistic regression, fuzzy logic and neural networks
Seibert J, Stendahl J, Sørensen R (2007) Topographical influences on soil properties in boreal forests. Geoderma 141:139–148. https://doi.org/10.1016/j.geoderma.2007.05.013
Soeters R, van Westen CJ (1996) Slope instability recognition, analysis, and zonation. In: Turner AK, Schuster RL (eds) Landslides, investigation and mitigation. National Academy, Washington D.C., pp 129–177
Steger S, Mair V, Kofler C et al (2021) Correlation does not imply geomorphic causation in data-driven landslide susceptibility modelling – Benefits of exploring landslide data collection effects. Sci Total Environ 776:145935. https://doi.org/10.1016/j.scitotenv.2021.145935
Sugiyama MT, de O, Gomes MCV (2023) Bacias hidrográficas Em Relevos escarpados: implicações Para a análise Da Suscetibilidade a corridas de Detritos. Revista Brasileira De Geomorfologia 24. https://doi.org/10.20502/rbg.v24i3.2269
Swets JA Measuring the accuracy of diagnostic systems. Science 240:1285-93., Teza TS, Guth G (1988) PL (2023) Hacking the topographic ruggedness index. Geomorphology 439:108838. https://doi.org/10.1016/j.geomorph.2023.108838
Szymanski FD et al (2022) Análise de inundações Em Bacias Montanhosas no Sul do Brasil Por Meio de Monitoramento e modelagem. Revista Brasileira De Geografia Física v15(n3):1564–1582. https://doi.org/10.26848/rbgf.v15.3.p1564-1582
UN – United Nations (2018) The 2030 agenda and the sustainable development goals: an opportunity for Latin America and the Caribbean. United Nations, Santiago
Vakhshoori V, Zare M (2018) Is the ROC curve a reliable tool to compare the validity of landslide susceptibility maps? Geomatics. Nat Hazards Risk 9:249–266. https://doi.org/10.1080/19475705.2018.1424043
Valdati J (2000) Riscos e desastres naturais: área de risco de inundação na sub-bacia do rio da pedra - Jacinto Machado/SC. Dissertation, Federal University of Santa Catarina
Valdati J, Ferreira DR, Villaça Gomes MC (2021) Determinação do Perigo de inundação a partir do Mapeamento Geomorfológico de Detalhe. Geosul 36:496–515. https://doi.org/10.5007/2177-5230.2021.e67385
Van Westen CJ (1993) Application of Geographical Information Systems to landslide hazard zonation. Thesis, University of Twente

Van Westen CJ, Castellanos E, Kuriakose SL (2008) Spatial data for landslide susceptibility, hazard, and vulnerability assessment: an overview. Eng Geol 102:112–131. https://doi.org/10.1016/j.enggeo.2008.03.010
Vasconcellos SM et al (2021) Flood hazard mapping in alluvial fans with computational modeling. Water Resour Manage 35:1463–1478. https://doi.org/10.1007/s11269-021-02794-7
Vieira BC, Fernandes NF, Augusto Filho O et al (2018) Assessing shallow landslide hazards using the TRIGRS and SHALSTAB models, Serra do mar, Brazil. Environ Earth Sci 77. https://doi.org/10.1007/s12665-018-7436-0
Wildner W, Ramgrab GE, Lopes RC et al (2008) Geologia e recursos minerais do estado do Rio Grande do Sul. Rigeo. https://rigeo.sgb.gov.br/handle/doc/10301
Wildner W, Camozzato E, Toniolo JA et al (2014) Mapa geológico do estado de Santa Catarina. Rigeo. https://rigeo.sgb.gov.br/handle/doc/17996
Yin KL, Yan TZ (1988) Statistical prediction models for slope instability of metamorphosed rocks. Proceedings of the 5th International Symposium on Landslides, Lausanne, 2: 1269–1272
Zêzere JL, Pereira S, Melo R et al (2017) Mapping landslide susceptibility using data-driven methods. Sci Total Environ 589:250–267. https://doi.org/10.1016/j.scitotenv.2017.02.188
Zhang Y (2011) Texture-Integrated classification of urban treed areas in high-resolution color-infrared imagery. Photogramm Eng Remote Sens 67:1359–1365
Zhang X, Lei Li, Xu C (2022) Large-scale landslide inventory and their mobility in Lvliang city, Shanxi province, China. Nat Hazards Res 2:111–120. https://doi.org/10.1016/J.NHRES.2022.05.002
Zhang Y, Chen N, Liu M et al (2020) Debris flows originating from colluvium deposits in Hollow regions during a heavy storm process in taining, southeastern China. Landslides 17:335–347. https://doi.org/10.1007/s10346-019-01272-x

Authors and Affiliations

Marina Tamaki de Oliveira Sugiyama[1] · José Eduardo Bonini[1] · Tiago Damas Martins[2] · Maria Carolina Villaça Gomes[3] · Susana Pereira[4,5] · Bianca Carvalho Vieira[1]

✉ Marina Tamaki de Oliveira Sugiyama
marinatamaki@usp.br

José Eduardo Bonini
jose.bonini@usp.br

Tiago Damas Martins
td.martins@unifesp.br

Maria Carolina Villaça Gomes
mcarolvg@gmail.com

Susana Pereira
sspereira@letras.up.pt

Bianca Carvalho Vieira
biancacv@usp.br

1 Department of Geography, University of São Paulo, Avenida Professor Lineu Prestes, 338, Cidade Universitária, São Paulo State 05508000, Brazil

2 Department of Geography, Federal University of São Paulo (UNIFESP), Avenida Jacu-Pêssego 2630, São Paulo State 08260001, Brazil

3 Department of Geography, State University of Rio de Janeiro (UERJ), Rua São Francisco Xavier, 524, Rio de Janeiro State 20550013, Brazil

4 Centre of Studies in Geography and Spatial Planning, Geography Department, Faculty of Arts and Humanities, University of Porto (UPorto), Via Panorâmica, s/n, Porto 4150-564, Portugal

5 Center of Geographical Studies, Institute of Geography and Spatial Planning, University of Lisbon (ULisboa), Rua Branca Edmée Marques, Edifício IGOT, Lisboa 1600-276, Portugal